Non-radial motion of eruptive filaments

B.P. Filippov and A.V. Lozhechkin
Institute of Terrestrial Magnetism, Ionosphere and Radio Wave Propagation, Russian Academy of Sciences, Troitsk Moscow Region 142190 Russia (bfilip@izmiran.troitsk.ru)

N. Gopalswamy
The Catholic University of America, Department of Physics, Washington DC 20064, USA (gopals@fugee.gsfc.nasa.gov)

Abstract. We develop a simple model to explain the nonradial motion of eruptive solar filaments under solar minimum conditions. The global magnetic field is derived from the first and third components of the spherical harmonic expansion of a magnetic scalar potential. The filament is modeled as a toroidal current located above the mid-latitude polarity inversion line. We investigate the stability of the filament against changes in the filament current and attempt to explain the nonradial motion and acceleration of the eruptive filament. We also discuss the limitations of this model.

1. Introduction

The large-scale solar magnetic field is known to have a strong influence on the early propagation of coronal mass ejections (CMEs) in the inner corona (Gopalswamy, Hanaoka, and Hudson, 2000; Gopalswamy and Thompson, 2000) as well as in the solar wind (Crooker, 2000). Under solar minimum conditions, observations from inner coronal imagers and white light coronagraphs show a non-radial motion of CMEs during their early life, followed by a radial propagation in the outer corona. In particular, the prominence core of CMEs has a non-radial trajectory in the early phase, followed by a radial trajectory later on. The nonradial motion is consistent with a statistical investigation by Plunkett *et al.* (2000) who showed a bimodal distribution for the near-surface location of the eruption (obtained from EUV observations) as compared to the equatorial position angle for the associated white light CMEs. A well-observed non-radial motion was recently reported by Gopalswamy, Hanaoka, and Hudson (2000): the white light CME of 14 December 1997 moved radially at a position angle of $\sim 91^\circ$ while the filament erupted from a position angle of $\sim 120^\circ$. During the non-radial motion, the filament showed an acceleration of ~ 1.4 m s^{-2} towards the equator and the speed was relatively small (~ 27 km s^{-1}). Based on the available images, the final CME speed in the sky plane was estimated as 570 km s^{-1} (Gopalswamy, Hanaoka, and Hudson, 2000).

In this paper, we develop a simple model to explain the nonradial motion of the filament under solar minimum conditions. A similar, but analytical model was studied recently by Lin *et al.* (1998) to find the equilibrium conditions with the inclusion of the curvature force. They used the boundary condition at the photosphere represented by a field equivalent to that produced by a point dipole at the center of the Sun and assumed the flux rope to be located at the equatorial plane. In the present work, we consider a more complicated field structure with three neutral lines one of them being at the equatorial plane as in Lin *et al.* (1998). Another important difference is that we solve the the equations of motion numerically to obtain the trajectory of the flux rope in the corona while Lin *et al.* (1998) do not consider the dynamics of the flux rope. We do not take into account possible formation of a current sheet below the flux rope studied by Lin and Forbes (2000) for a model with translational symmetry assuming that reconnection occurs at a sufficiently rapid rate to allow the flux rope to escape without substantial deceleration.

2. Model

We consider a simple model of the filament equilibrium in the solar global magnetic field. We shall use axial symmetry and assume the filament to be a ring current I or a toroidal flux rope lying in the latitudinal plane above the photospheric polarity inversion line. At solar minimum, there are typically three global polarity inversion lines: one of them is located at the equator and the other two are located at middle latitudes in the northern and southern hemispheres, respectively. This configuration can be modeled by the third spherical harmonic in the expansion of a magnetic scalar potential

$$u = \sum_i \frac{A_i}{r^{i+1}} P_i\left(\frac{z}{r}\right) \ . \tag{1}$$

Here A_i are coefficients of the multipolar expansion in Legendre polynomials, P_i , $r = \sqrt{\rho^2 + z^2}$; ρ and z are the coordinates of the cylindrical coordinate system centered at the sun with the z-axis along the solar rotation axis (in the north direction). Since the solar minimum corona reveals a bipolar form, the first harmonic should also be included with some weight. Differentiating Equation (1) with respect to ρ and z one can obtain ρ and z-components of the global magnetic field

$$B_\rho^{(ph)} = 3\, A_1 \frac{\rho z}{r^5} + A_3 \frac{5(4\rho z^3 - 3\rho^3 z)}{2\, r^9} \ , \tag{2}$$

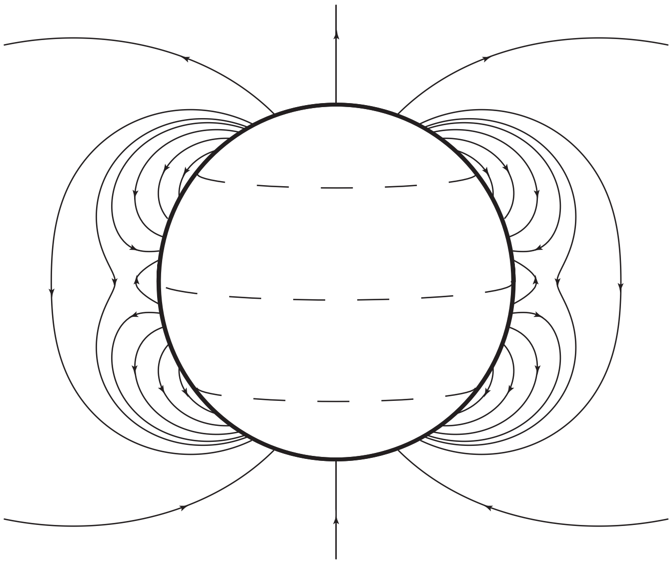

Figure 1. Field lines of the solar global magnetic field in a meridional plane ($\varphi =$ const) used in the model. The dashed lines show three polarity inversion lines of the global magnetic field in the solar minimum. The large solid circle represents the photosphere of the Sun.

$$B_z^{(ph)} = A_1 \frac{2z^2 - \rho^2}{r^5} + A_3 \frac{3\rho^4 - 24\rho^2 z^2 + 8z^4}{2\, r^9} \,. \tag{3}$$

Figure 1 shows the global magnetic field. The relationship between the first and third harmonic coefficients (A_1 and A_3) defines the height of the neutral line in the corona. In units of solar radii ($R_\odot$) the height of the neutral line ξ is

$$\xi = \frac{1}{R_\odot} \sqrt{\frac{3}{2} \frac{A_3}{A_1}} \,. \tag{4}$$

We assume that the filament is located at the neutral line in the southern hemisphere. We represent the filament by a current ring (or flux rope) with a total current I (see Figure 2).

The curvature of the flux rope creates an outward force. The force per unit length on the filament f_I, which stretches the current ring is given by (Shafranov, 1966),

$$f_I = \frac{I^2}{c^2\rho}\left(\ln\frac{8\rho}{a} - \frac{3}{2} + \frac{l_i}{2}\right) , \tag{5}$$

where ρ is the major radius of the torus (filament), a is its minor radius and l_i is the internal self-inductance per unit length of the current tube. This formula is valid under assumption $\rho \gg a$, which is reasonable for a filament with a length much greater than its cross section. We will not consider here the dynamics of the minor radius a because, with $\rho \gg a$, the assumed internal pressure and axial magnetic field are able to support the equilibrium along the minor radius. We can assume the current density to be uniform inside the tube, which gives $l_i = 1/2$, or follow Lin et al. (1998) and assume the magnetic field to be force-free inside the flux rope, which yields $l_i = 1$. The difference would not be very significant as $\rho \gg a$. So Equation (5) becomes

$$f_I = \frac{I^2}{c^2\rho}\left(\ln\frac{8\rho}{a} - 1\right) . \tag{6}$$

The photospheric plasma is dense and a good conductor so that it prevents the penetration of the magnetic fields due to the coronal current into the sun's interior. The surface of the photosphere serves as a spherical mirror for the ring magnetic field. The situation is analogous to the mirror charge in electrostatics: for a charge at a distance r_1 from the center of a sphere, the image charge is located at a distance r_2 on the line connecting the charge with the center of the sphere, given by, $r_2 = R^2_{sphere}/r_1$, where R_{sphere} is the radius of the sphere. The value of the mirror charge is $e_2 = e_1\sqrt{r_2/r_1}$. For a ring current reflection, the value of the mirror current I_m should be increased by a factor $r_1/r_2 = \rho/\rho_m$ due to the different lengths of the coronal and mirror currents. So, this gives

$$\rho_m = \frac{R^2_\odot \rho}{\rho^2 + z^2}, \quad z_m = \frac{R^2_\odot z}{\rho^2 + z^2}, \quad I_m = -I\frac{\sqrt{\rho^2 + z^2}}{R_\odot} , \tag{7}$$

where z_m is the z-coordinate of the mirror current ring.

The magnetic field generated by the current ring is given by (Landau, Lifshitz, and Pitaevsky, 1984)

$$\begin{aligned} B_\rho^{(m)} &= \frac{2\,I_m}{c}\frac{(z - z_m)}{\rho\sqrt{(\rho_m + \rho)^2 + (z - z_m)^2}} \\ &\times \left[-K(k) + \frac{\rho_m^2 + \rho^2 + (z - z_m)^2}{(\rho_m - \rho)^2 + (z - z_m)^2}E(k)\right] , \end{aligned} \tag{8}$$

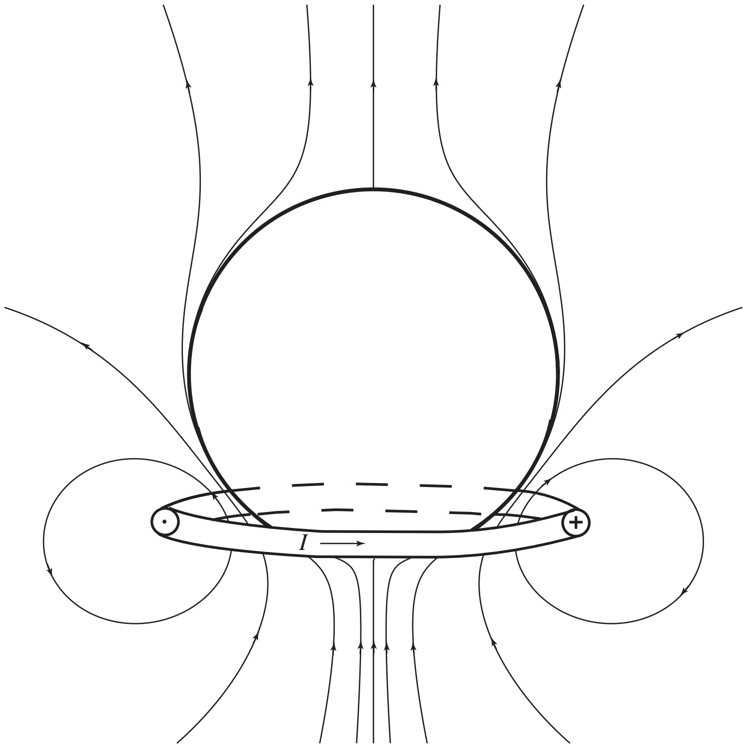

Figure 2. Field lines of the filament and mirror currents in a meridional plane. Toroidal flux rope with the total current I is located above the photospheric polarity inversion line in southern hemisphere.

$$B_z^{(m)} = \frac{2\,I_m}{c} \frac{1}{\sqrt{(\rho_m + \rho)^2 + (z - z_m)^2}} \times \left[K(k) + \frac{\rho_m^2 - \rho^2 - (z - z_m)^2}{(\rho_m - \rho)^2 + (z - z_m)^2} E(k) \right] , \tag{9}$$

where

$$k^2 = \frac{4\rho_m \rho}{(\rho_m + \rho)^2 + (z - z_m)^2} , \tag{10}$$

$K(k)$, $E(k)$ are the complete elliptic integrals of the first and second kinds, respectively. Figure 2 shows the field lines of the filament and mirror currents. It is seen that no field line penetrates the solar surface.

The equation of filament motion can be written in terms of the forces acting on unit length of the filament. In the cylindrical coordinates, the

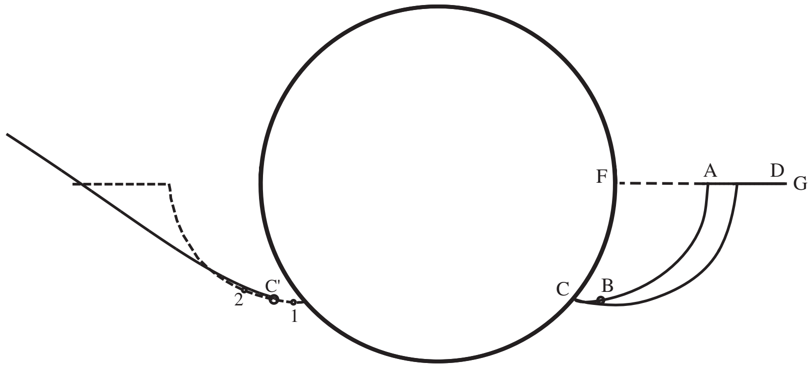

Figure 3. Locus of the equilibrium point of the filament in the $\rho - z$ plane. The open circle marked C′ corresponds to the point where the filament current reaches its critical value. When the filament is at point 1, it is stable, while it is unstable at point 2. The curve GF corresponds to a filament in the equatorial plane (not considered here). The segment AG is considered here. C is the lowest height of the filament where the current has zero value. B corresponds to the minimum value of A_1. The curves AD, AB and CD are discussed in the text. The initial part of the trajectory of the erupting filament is also shown in the left hand side of the figure.

equation of motion is given by,

$$m\frac{d^2\rho}{dt^2} = \frac{I}{c}(B_z^{(ph)} + B_z^{(m)}) + f_I - mgR_\odot^2 \frac{\rho}{(\rho^2 + z^2)^{3/2}} , \qquad (11)$$

$$m\frac{d^2 z}{dt^2} = -\frac{I}{c}(B_\rho^{(ph)} + B_\rho^{(m)}) - mgR_\odot^2 \frac{z}{(\rho^2 + z^2)^{3/2}} , \qquad (12)$$

where $\mathbf{B}^{(ph)}$ is the magnetic field of the photospheric sources given by Equations (2) and (3), $\mathbf{B}^{(m)}$ is the magnetic field of the mirror current given by Equations (8) and (9), m is the mass of the filament per unit length, and g is the free-fall acceleration at the photospheric level.

3. Model Calculations

3.1. Equilibrium

We specify all the parameters that enter into Equations (11) and (12) and then solve them with zero left-hand sides in order to find the initial equilibrium position. Let $\xi = 1.2$ and magnetic field strength $B \sim 1$ G in the corona near the filament. Then $A_1 = 6 \times 10^{32}$ G cm^3, and $A_3 = 2.8 \times 10^{54}$ G cm^5. The typical mass per unit length of the filament $\sim 10^5$ g cm^{-1}. We also let the initial value of the electric current in the ring to be $I \sim 10^{11}$ A, which is typical for filament currents (Ballester, 1984; Vrsnak et al., 1988; Kulikova et al., 1989; Srivastava, Ambastha, and Bhatnagar, 1991). To obtain a stable equilibrium near the polarity inversion line we should choose the same signs for A and I. In this case, the force $\mathbf{I} \times \mathbf{B}^{(ph)}$ restores the filament to the inversion line.

The dashed curve on the left hand side of Figure 3 shows the line at which the filament is in equilibrium state, given by the solution of Equations (11) and (12) with the zero left hand side, and using the current value I as a parameter. This is not an evolution curve as, for instance, in Figure 5 of Isenberg et al. (1993). Each point of the curve corresponds to a different flux rope to be inserted into the coronal magnetic field with its specific value of the current. The height of the equilibrium point above the photosphere is given by $h = (\sqrt{\rho^2 + z^2} - R_\odot)$. The dependence of h on the magnitude of the current is shown in Figure 4 (the height h and all the distances in the following plots are in the units of solar radius $R_\odot$). Note that there are two equilibrium points corresponding to each value of the current. When the current increases, the height of the lower point also increases while the height of the upper point decreases. They merge when the current value reaches the critical value I_c. This critical point (C$'$) is marked with an open circle on the equilibrium curve in Figure 3. The height of the critical

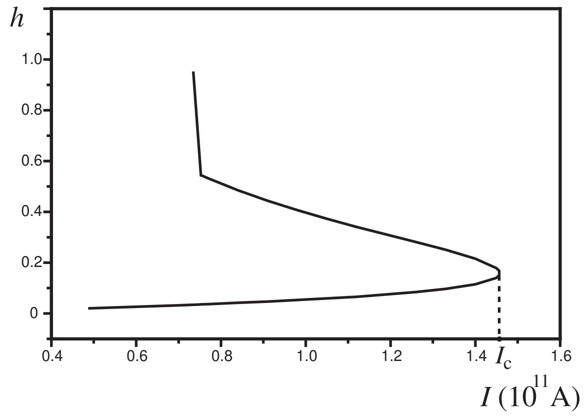

Figure 4. The dependence of the height of the equilibrium point above the photosphere h on the current magnitude I. h is in the units of solar radii $R_\odot$. Note that there are two values of h for each value of $I < I_c$.

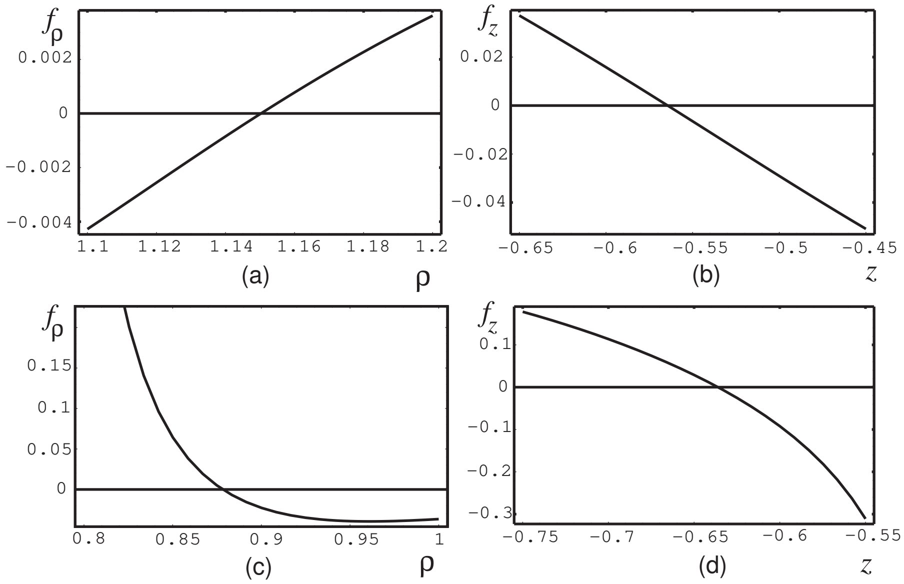

Figure 5. The behavior of the f_ρ and f_z force components, near the equilibrium point 2 above the critical height (a), (b) and near the equilibrium point 1 below (c), (d) the critical height. The forces are in the units of 7×10^{10} dyne.

point above the limb is about $0.17R_\odot$. The equilibrium is stable only below the critical point. Figure 5 shows the behavior of the right hand sides of the equations of motion near the equilibrium positions (ρ_1, z_1) and (ρ_2, z_2) located just below and above the critical point. $f_\rho(\rho, z)$ is set equal to the right-hand side of Equation (11) and $f_z(\rho, z)$ to that of Equation (12) (taking into account Equation (13)).

Figures 5(a) and (c) show the ρ-dependence of $f_\rho(\rho, z_{1,2})$ with the fixed $z = z_{1,2}$ while Figures 5(b) and (d) show the z-dependence of $f_z(\rho_{1,2}, z)$ with the fixed $\rho = \rho_{1,2}$. It is evident that the filament has a stable equilibrium in the z direction because the force f_z at larger values of negative z is positive and at smaller values of negative z is negative. So it brings the filament to the equilibrium position. In the ρ direction, the lower point 1 is stable (the force f_ρ at larger values of ρ is negative and at smaller values of ρ is positive) while the higher point 2 is unstable (the signs of f_ρ are opposite). This is similar to the case with the straight line current model (Molodensky and Filippov, 1987).

For finite displacements of the filament we should take into account the changes on the current due to inductance. It has the form of conservation of the magnetic flux through the filament ring:

$$\Phi = \Phi_{ph} + LI = \text{constant} , \tag{13}$$

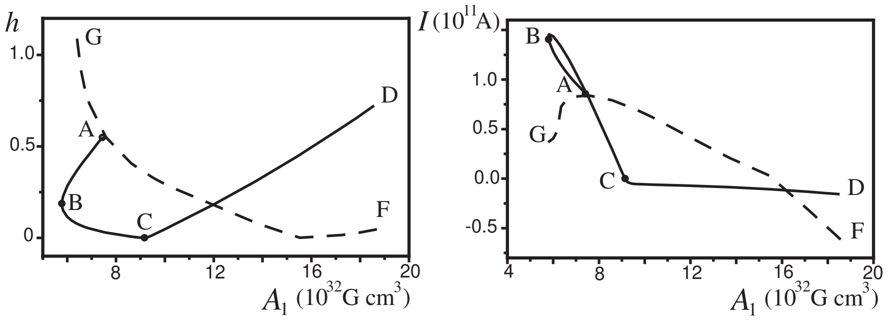

Figure 6. The dependence of the filament height above the photosphere h (left) and the filament current I (right) on the scale coefficient of the global magnetic field, A_1. The total magnetic flux through the ring $\phi = 7.2 \times 10^{22}$ Mx was chosen to obtain the critical value of the filament current $I_c = 1.5 \times 10^{11}$ A.

where

$$L = 4\pi\rho \left(\ln\frac{8\rho}{a} - \frac{3}{2} \right) \tag{14}$$

is the self-inductance of the ring current of major radius ρ and minor radius a (Landau, Lifshitz, and Pitaevsky, 1984). For the photospheric flux Φ_{ph} the following integration should be performed

$$\Phi_{ph} = 2\pi \int_0^\rho B_z^{(ph)} \rho\prime \, d\rho\prime \ . \tag{15}$$

Substituting Equations (2) and (3) into Equation (15) we find

$$\Phi_{ph} = 2\pi A_1 \frac{\rho^2}{(\rho^2 + z^2)^{3/2}} - 2\pi A_3 \frac{\rho^4 - 4\rho^2 z^2}{2(\rho^2 + z^2)^{7/2}} \ . \tag{16}$$

The inductance equation is very important on short time intervals, for instance, during an eruption. During the long pre-eruptive stage, this equation cannot be very rigorous due to finite electric conductivity and some other reasons that allow the formation of a current in the corona.

Simultaneous solution of Equations (11) - (13) gives us the evolution curves of a filament when the external magnetic field is changing. As the filament current can change in accordance with the magnetic flux conservation, we obtain complicated equilibrium curves. Equilibrium positions are shown in the right hand side of Figure 3. Figure 6 shows the dependence of the filament height above the photosphere h and the filament current I on the scale coefficient of the global magnetic field A_1. Points A, B, C, D, F, G indicate the different peculiarities in the evolution curves. The curve GF corresponds to the location of the filament in the equatorial plane. For our analysis, we are interested only in the branch AG above the neutral point. There is a stable equilibrium along this branch (below some reasonable height) but it cannot be realized in the present case of a filament located originally at middle latitudes. This is due to the kinetic energy of the filament (see below). Point C is the lowest position of the filament just above the photospheric surface with a zero value of the current. Point B corresponds to the minimum value of A_1 (see Equation (1)). The value of the current I does not reach the maximum at this point, which is in agreement with the results of Forbes and Isenberg (1991), Isenberg, Forbes, and Demoulin (1993), Forbes and Priest (1995). However, the deviation from the maximum current value is very small (about 1%). Branch BC is the only stable portion of the curve AD. Branch AB is unstable for ρ-displacements, while the branch CD corresponding to the negative current is unstable for z-displacements. In response to the change of the global field (described by A_1 and A_3), the evolution of the system along the curve segment C $\rightarrow$ B is quasi-static until the point B is reached; any further evolution must be dynamic. Point B constitutes the so-called critical point, and this curve explicitly indicates that a catastrophic loss of equilibrium of the system occurs at point B during evolution. This is exactly the situation that has extensively been discussed by many authors since the seventies when Van Tend and Kuperus (1978) raised the original idea for the catastrophic models of solar eruptions.

3.2. Eruption

We now turn to the numerical solution of the equations of motion. When a deviation from the equilibrium occurs, the filament will oscillate near the equilibrium point. If we add some artificial dissipation $-k_d\mathbf{v}$ (k_d is the dissipation coefficient and $\mathbf{v}$ is the velocity) to the right hand sides of Equations (11) and (12), the filament will come to equilibrium state after a number of damped oscillations (Figure 7).

Figure 8 shows the trajectory of the erupting filament after its current has been increased by about 2 % over the critical value. The initial part of the trajectory is also shown in the left hand part of Figure 3 as a solid line originating near the critical point C$'$. After the loss of equilibrium, the filament moves up and towards the equatorial plane. At $\rho = 2.7$ it crosses the equatorial plane and moves further in the direction tilted at an angle $\sim 20°$ to this plane. Figure 9(a) shows the plot of ρ and z against time t. The speed of the filament changes slowly within the first hours and then quickly increases to approach a constant value within the following two hours (Figure 10). This behavior is consistent with the nonradial filament motions during CMEs. The filament current falls by a factor of two before the filament reaches the equatorial plane and then decreases more gradually (Figure 9(b)).

As we expect the beginning of the eruption to be due to the loss of filament equilibrium near the critical point, the values of external magnetic field (defined by A_1) and electric current I are related one another. There remains only one free parameter to describe the different dynamics of the eruption. This is the mass m of the filament. The filament equilibrium is only slightly affected by the gravitational force. For instance at the point 1 in Figure 3, the gravity is less than 2 % of the magnetic force. However, the mass as an inertia measure is very significant for the dynamics and kinematics of an eruption. To obtain the observed final speed of 500 km s^{-1} for the filament in Figure 10 we choose the mass per unit length 0.75×10^6 g cm^{-1}. This is the inertia that does not allow the filament to stop in the equilibrium position on the branch AG of the evolution curve in the equatorial plane. The filament gains rather high kinetic energy and cannot be stopped by the weak bipolar magnetic field.

4. Conclusions

We analyzed the reasons for the nonradial motion of eruptive prominences. The 1997 December 14 filament eruption (Gopalswamy, Hanaoka, and Hudson, 2000) is a clear example of such a behavior. We developed a simple model to explain the nonradial motion of eruptive solar filaments under solar minimum conditions. The filament is modeled as a toroidal current located above the mid-latitude polarity inversion line. The speed profile in Figure 10 shows that the filament is ascending rather slowly just after the beginning of the catastrophic process. The

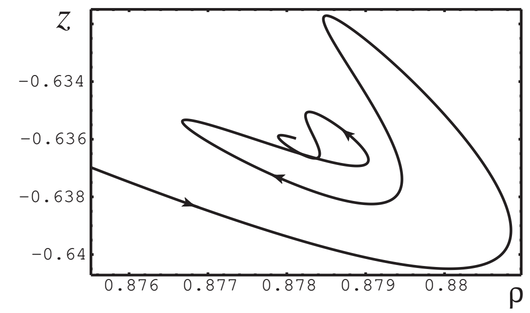

Figure 7. Damped oscillations of the filament near the stable equilibrium point 1. $k_d = 1.2$.

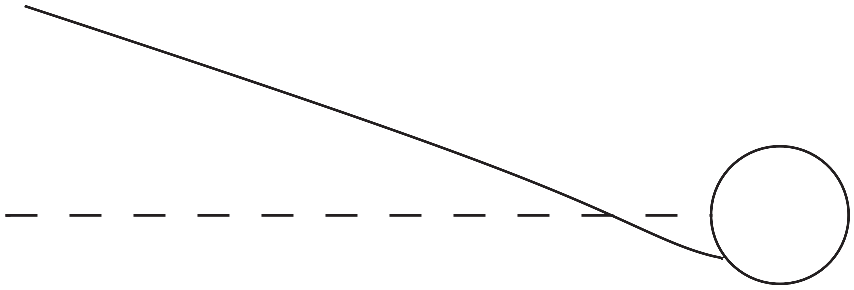

Figure 8. The trajectory of the erupting filament in the $\rho - z$ plane.

main acceleration takes place more than an hour after the start of the eruption. The trajectory of the filament is not radial but is tilted toward the equatorial plane at a small angle. This is the guiding action of the coronal magnetic field on the current motion. Such motion could produce the ‘swelling’ in the southern part of the overlying equatorial streamer. At large distances, the model predicts that the prominence and the surrounding CME move at a small angle to the equatorial plane.

Thus the model is able to explain most of the features of the non-radial prominence eruptions. We would like to point out that the model is not perfect and there is room for improvement. For example, the actual flux rope may not be a torus around the Sun, but is anchored in the photosphere. As we mentioned before the the final trajectory of the prominence makes a small angle with the equatorial plane. This is not completely consistent with the observation that the CME propagates along the equatorial plane. The discrepancy may be due to the oversimplification of the coronal magnetic field, particularly at large

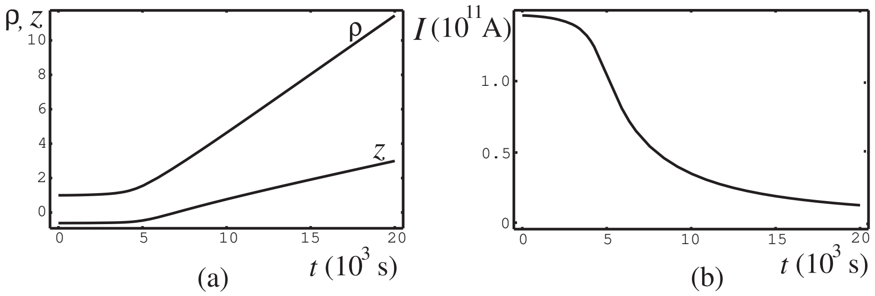

Figure 9. The dependence of the filament coordinates ρ, z (a) and the filament current I (b) on time.

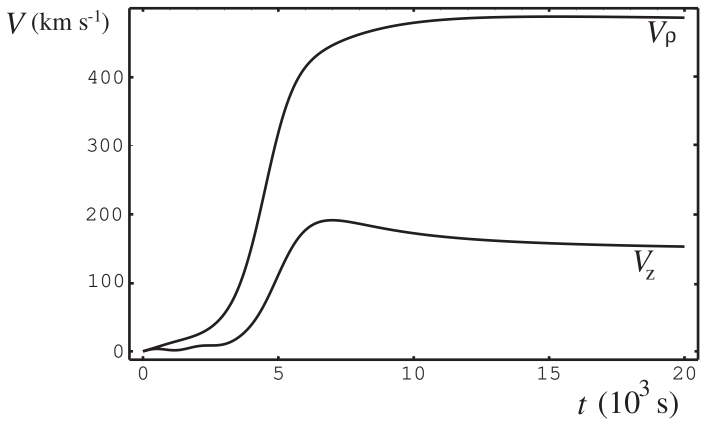

Figure 10. The speed of the filament as a function of time.

distances where the field should be more radial because of the action of the solar wind.

Acknowledgements

The authors would like to thank the anonymous referee for helpful comments and suggestions. The work of BPF and AVL was supported in part by Russian Foundation for Basic Research (grant 00-02-17736) and Russian State Astronomical Program. NG was supported by NASA (NAG5-6139, NCC5-8998 and the ISTP/SOLARMAX program), Air Force Office of Scientific Research (F49620-00-1-0012) and NSF (ATM9819924).

References

Ballester, J.L.: 1984, *Solar Phys.* **94**, 151.
Crooker, N.: 2000, *J. Atmospheric Terrestr. Phys.* **62**, 1071.
Forbes, T.G. and Isenberg, P.A.: 1991, *Astrophys. J.* **373**, 294.
Forbes, T.G. and Priest, E.R.: 1995, *Astrophys. J.* **446**, 377.
Gopalswamy, N., Hanaoka, Y., and Hudson, H.S.: 2000, *Adv. Space Res.* **25**, No. 9, 1851.
Gopalswamy, N. and Thompson, B. J.: 2000, *J. Atmospheric Terrestr. Phys.*, **62**, 1457.
Isenberg, P.A., Forbes, T.G., and Demoulin, P.: 1993, *Astrophys. J.* 417, 368.
Kulikova, G.N., Molodensky, M.M., Starkova, L.I., and Filippov, B.P.: 1989, in R.B. Teplitskaya (ed.) *Solar Magnetic Fields and Corona* **2**, Nauka, Novosibirsk, p. 156.

Landau, L.D., Lifshitz, E.M., and Pitaevsky, L.P.: 1984, *Electrodynamics of Continuos Media*, 2nd edition, Pergamon Press, Oxford.
Lin, J. and Forbes, T.G.: 2000, *J. Geophys. Res.* **105**, 2375.
Lin, J., Forbes, T.G., Isenberg, P.A., and Demoulin, P.: 1998, *Astrophys. J.* **504**, 1006.
Molodensky, M.M. and Filippov, B.P.: 1987, *Soviet Astron.* **31**, 564.
Plunkett, S. P., Thompson, B. J., St. Cyr, O. C., and Howard, R. A.: 2000, *J. Atmospheric Terrestr. Phys.* **63**, 389.
Shafranov, V.D.: 1966, in M.A. Leontovich (ed.) *Reviews of Plasma Physics*, Vol. **2**, Consultants Bureau, New York, p. 103.
Srivastava, N., Ambastha, A., and Bhatnagar, A.: 1991, *Solar Phys.* **133**, 339.
Van Tend, W. and Kuperus, M.: 1978, *Solar Phys.* **59**, 115.
Vrsnak, B., Ruzdjak, V., Brajsa, R., and Dzubar, A.: 1988, *Solar Phys.* **116**, 45.